ORIGINAL ARTICLE

Cytometry PART A
Journal of the International Society for Advancement of Cytometry

High-Precision Characterization of Individual *E. coli* Cell Morphology by Scanning Flow Cytometry

Anastasiya I. Konokhova,[1,2] Andrey A. Gelash,[2] Maxim A. Yurkin,[1,2] Andrey V. Chernyshev,[1,2] Valeri P. Maltsev[1,2]*

[1]Institute of Chemical Kinetics and Combustion SB RAS, 630090 Novosibirsk, Russia

[2]Physics Department, Novosibirsk State University, 630090 Novosibirsk, Russia

Received 27 August 2012; Revision Received 25 February 2013; Accepted 15 March 2013

Grant sponsor: Program of the Russian Government "Research and Educational Personnel of Innovative Russia"; Grant numbers: P1039, P422, 14.740.11.0921, 8752, 14.B37.21.1972, 14.A18.21.2009, 8804; Grant sponsor: Government of Russian Federation; Grant number: 11.G34.31.0034; Grant sponsor: Program of the President of the Russian Federation for State Support of the Leading Scientific Schools; Grant number: NSh-65387.2010.4; Grant sponsor: Russian Foundation of Basic Research; Grant numbers: 12-04-00737-a, 12-04-31083; Grant sponsor: EU Marie Curie Project; Grant number: PIRSES-GA-2010-269156-LCS; Grant sponsor: Stipend of the President of Russian Federation for Young Scientists.

*Correspondence to: Valeri P. Maltsev, Institute of Chemical Kinetics and Combustion SB RAS, Institutskaya 3, 630090 Novosibirsk, Russia

Email: maltsev@kinetics.nsc.ru

Published online 8 April 2013 in Wiley Online Library (wileyonlinelibrary.com)

DOI: 10.1002/cyto.a.22294

Abstract

We demonstrate a flow-cytometric method to measure length and diameter of single *Escherichia coli* cells with sub-diffraction precision. The method is based on the original scanning flow cytometer that measures angle-resolved light-scattering patterns (LSPs) of individual particles. We modeled the shape of *E. coli* cells as a cylinder capped with hemispheres of the same radius, and simulated light scattering by the models using the discrete dipole approximation. We computed a database of the LSPs of individual bacteria in a wide range of model parameters and used it to solve the inverse light-scattering problem by the nearest-neighbor interpolation. The solution allows us to determine length and diameter of each individual bacterium, including uncertainties of these estimates. The developed method was tested on two strains of *E. coli*. The resulting precision of bacteria length and diameter measurements varied from 50 nm to 250 nm and from 5 nm to 25 nm, respectively. The measured distributions of samples over length and diameter were in good agreement with measurements performed by optical microscopy and literature data. The described approach can be applied for rapid morphological characterization of any rod-shaped bacteria. © 2013 International Society for Advancement of Cytometry

Key terms

E. coli; light scattering; inverse light-scattering problem; scanning flow cytometry; discrete dipole approximation

LIGHT scattering, as it was first proposed and substantiated by Wyatt in 1968 (1), is a powerful physical method for bacteria identification and characterization (2–4). The intensity, polarization, and spatial distribution of light scattering by a particle depend on the overall particle morphology, including shape, internal distribution of the refractive index, and the particle orientation relative to the incident beam. Therefore, spatial distribution, i.e., angular dependence of light-scattering intensity provides valuable information on morphological properties of a particle (5). Under certain a priori assumptions, the morphology information can be used to identify microorganisms (distinguish them among several classes) and can also provide a real-time monitoring of bacterial growth (6). Moreover, light-scattering can be used in combination with other (e.g., fluorescent) methods to correlate morphological changes with cell cycle phases. However, the utility of any light-scattering method for this application largely depends on the precision of morphology assessment, e.g., of single-bacteria length measurement.

Angle-resolved light scattering was applied by many researchers in studies of bacterial cells, both on bacteria suspensions and single cells. The angular dependence of light scattered by suspension of spherical *Staphylococcus albus* was measured with "Differential I" light-scattering photometer, which agreed with calculations using the Mie theory (7). The measurements of the light scattering from randomly oriented heterogeneous cultures of *E. coli* in water were carried out with a special photometer

in the angular range from 10° to 90° (8). The Rayleigh-Debye approximation applied to the homogeneous ellipsoid correctly predicted the observed positions of scattering minima. Bronk et al. (9) measured combinations of Mueller matrix elements for a randomly oriented suspension of *E. coli* in the scattering angles ranging from 10° to 150°, which were demonstrated to be in a good agreement with calculations performed using the coupled dipole approximation for cells modeled by a cylinder capped with hemispheres (10). In combination with measurements of the cell volume by Coulter method, they demonstrated rapid determination of both average diameter and average lengths of bacterial population (11).

Sequential analysis of individual cells generally provides better accuracy of characterization of population in comparison to measurement of whole cell suspension. The most powerful light-scattering technique for analysis of multiple individual bacteria is flow cytometry (12–14). An ordinary flow cytometer allows one to measure only two numbers from light scattering which are the intensities of forward scatter (FSC) and side scatter (SSC). However, the relationship between cell morphology and these two parameters is generally so complicated that little hope is left for a detailed characterization of bacterial population. This is exemplified by Müller and Nebe-von-Caron (15), who recently reviewed the problems with the flow cytometric analysis of bacterial cells. With regards to light scattering, they also stated that "the performance of most cytometers is insufficient to analyze the small differences in the signals or to obtain any signal at all due to lack of critical alignment and instrument noise." These factors become critical, because the ordinary FSC and SSC light-scattering signals per se are instrument-dependent in contrast to angle-resolved light scattering of individual bacteria.

A logical development of standard flow-cytometric is to measure a multiangle scattering or even an entire light-scattering pattern (LSP) of individual particles in a wide angular range. The authors (16,17) performed differentiation of four different bacterial species using multiangle (four-ring) FSC flow cytometer. The measurement of the LSP was realized with the scanning flow cytometer (SFC) (18,19). There was shown that LSPs are very sensitive to a particle morphology, i.e., physical dimensions and consistence, as well as to an orientation of the particle within an incident laser beam. The high-sensitivity of LSPs to particle morphology improves cell identification from light scattering in flow cytometry substantially (20,21). Moreover, an analysis of the LSP potentially allows one to determine morphological characteristics of biological particles (5). However, such characterization constitutes the inverse light-scattering (ILS) problem, which is a field of active research, see e.g., Refs. 22 and 23.

LSPs of individual *E. coli* cells were first experimentally measured by Shvalov et al. (24) in logarithmic and stationary phases of cell growth. They demonstrated qualitative differences of LSPs between these two phases, but have not addressed the characterization problem due to unbearable computational complexity. However, a number of methods have since been developed for the solution of the ILS problem for a single particle. In particular, global optimization methods were used for robust characterization of single- and multilayered spheres, even with large experimental noise (22,25). Unfortunately, optimization is not feasible for nonspherical particles due to large computational cost of the direct light-scattering problem. This can be alleviated by using a preliminary calculated database of LSPs and solving the inverse problem by the nearest-neighbor interpolation. This approach was demonstrated for spheres (26), spheroids (27), and biconcave disks (28).

In this article, we studied light-scattering properties of individual *E. coli* cells. We developed a method to solve the ILS problem for individual rod-shaped bacteria, i.e., to characterize their morphology with the SFC, using a preliminarily calculated database of theoretical LSPs. The method itself is described in the "Materials and Methods" section, including standard sample preparation, measurements of LSPs with the SFC, database-based fit of experimental LSPs with theoretical ones, and uncertainties estimates. In the "Results" section, we illustrate the performance of this method on samples of two strains of *E. coli* and compare results to those obtained with the optical microscopy. Conclusion is given in the "Discussion" section.

Materials and Methods

Scanning Flow Cytometer

A detailed description of the SFC was given elsewhere (19). Here, we only briefly define the measured experimental signal. A 30 mW laser of 405 nm (Radius) was used for generation of LSP of individual particles. Another laser (660 nm, 30 mW) was used for generating trigger signal. The measured LSP is expressed as (19):

$$I(\theta) = \frac{1}{2\pi}\int_0^{2\pi} [S_{11}(\theta,\varphi) + S_{14}(\theta,\varphi)]\, d\varphi, \qquad (1)$$

where S is the Mueller matrix (29), and θ and φ are polar and azimuth scattering angles, respectively. The operational angular range of the SFC was determined from analysis of polystyrene microspheres, as described in (22) to be from 10° to 40°.

Optical Microscope

Images of *E. coli* cells were obtained with optical microscope Carl Zeiss Axio Imager.A1 using 100× oil immersion objective with 1.3 numerical aperture. The microphotographs were processed using MATLAB-based software package MicrobeTracker (30), capable to automatically measure bacteria dimensions from microscope images (default parameter set alg4ecoli.set was used). Typical processed image is shown in Figure 1—one can see that the largest bacteria are ignored by MicrobeTracker with current settings. We have not investigated this problem due to low number of such bacteria (<4%). However, it does truncate the tail of the measured distribution of sample over length.

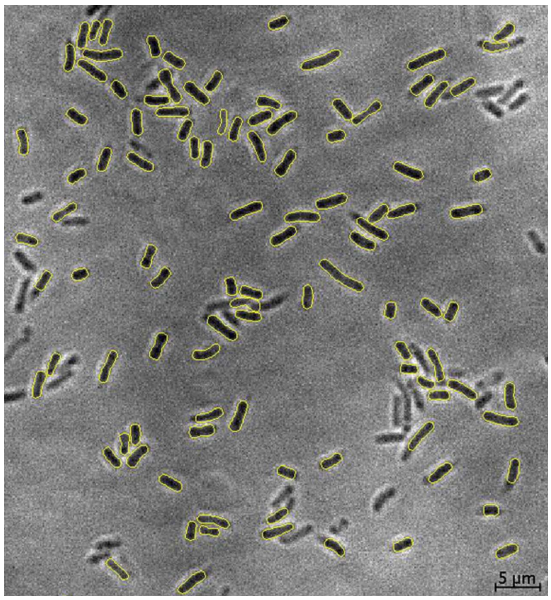

Figure 1. Typical microscope image of *E. coli* cells processed with MicrobeTracker. [Color figure can be viewed in the online issue which is available at wileyonlinelibrary.com.]

Cell Cultivation

The XL2-Blue (Stratagene) and XL10-GOLD (ATCC 55962) strains of *E. coli* were used in this work. The bacterial cells were grown at 37°C in a thermostat with vigorous shaking. The standard growth media LB (31) (10 g NaCl, 10 g tryptone, 5 g yeast extract, 1 L distilled water, pH 7.5) was used as a broth. After preparation, the medium was autoclaved at 120°C. Both used strains are resistant to ampicillin, so it was added to the medium in concentration 0.05 g/L for growth suppression of extraneous cells. No additional treatment of the sample was carried out before the experiments.

Optical Model of *E. coli* Cell

To simulate the scattering from the individual *E. coli* cells, we use an optical model of a cylinder capped with hemispheres of the same radius, previously used for simulation in (10) and based on microscopic analysis of *E. coli* cells. This model is described by three morphological parameters (length l, diameter d, and refractive index n) and an auxiliary parameter (orientation angle ψ of cell in the flow of the SFC). Deviations from this model are discussed in "Light Scattering by Dividing *E. coli* Cells" section.

Light Scattering Simulation

To simulate light-scattering by a single *E. coli* cell, we used the discrete dipole approximation (DDA), a general method to simulate light scattering by particles of arbitrary shape and composition (32). In particular, we used open-source code ADDA v.1.0 (33), which can run on a cluster of computers, parallelizing a single DDA computation. LSPs of *E. coli* cells [see Eq. (1)] were simulated for polar angle θ from 10° to 40° using default discretization of 10–11 dipoles per wavelength and step of 5.5° for integration over azimuthal angle φ. The refractive index of the medium (0.9% saline) is 1.337. We estimated accuracy of DDA simulations for six typical bacteria, comparing with DDA results using much finer discretization (40 dipoles per wavelength). Relative accuracy is better than 4% for any θ in the parts of the LSP, where intensity itself is significant, but is much worse for parts with negligibly small intensity. Nevertheless, the overall norm of the simulation error, defined as square root of S [Eq. (2)], is less than 3% of the LSP norm itself. All simulations were run on the compute cluster of Supercomputing center of the Novosibirsk State University (34). Typical simulation time of single LSP for average bacteria cell (0.6×6.2 μm) is 80 s on a single-core of Intel X5355 processor (2.66 GHz).

Light Scattering by Dividing *E. coli* Cells

The division of *E. coli* is known to be accompanied by formation of constriction in the middle of cell longer axis (35). To estimate the effect of cell division on LSPs and hence on the results of characterization, we compared LSPs of five different bacteria with and without constrictions. Here, we present only a single typical result in Figure 2. The difference between the two calculated LSPs is less than 10%, which leaves little hope to distinguish dividing from nondividing cells based on the noisy experimental LSPs. However, it also shows that our characterization algorithm ("Inverse Light-Scattering Problem" section) should be perfectly applicable to dividing cells. Thus, in the rest of the manuscript, we assume that dividing cells are characterized as a single cell with doubled length.

Inverse Light-Scattering Problem

To solve the ILS problem, we use a method previously developed in (22,23) and briefly describe it below. The problem is transformed into the global minimization of the weighted sum of squares:

$$S(\boldsymbol{\beta}) = \sum_{i=1}^{N} z_i^2,\ z_i = w(\theta_i)(I_{\text{th}}(\theta_i, \boldsymbol{\beta}) - I_{\text{exp}}(\theta_i)), \qquad (2)$$

where $\boldsymbol{\beta}$ is a vector of four model parameters, I_{th} and I_{exp} are theoretical and experimental LSP, respectively, $N = 64$ number

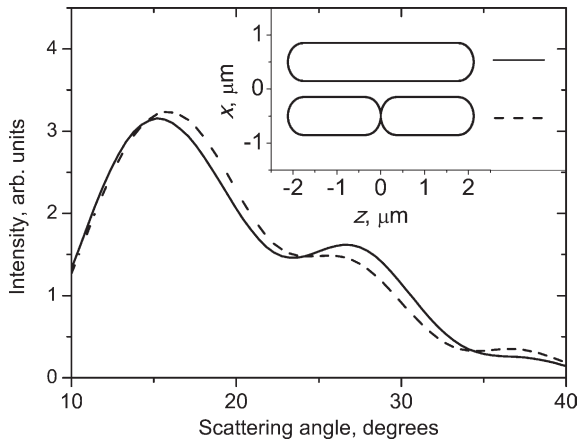

Figure 2. Comparison of theoretical light-scattering profiles for *E. coli* with and without constriction (shapes shown in the inset) with parameters $l = 4$ μm, $d = 0.7$ μm, $n = 1.40$, $\psi = 10°$.

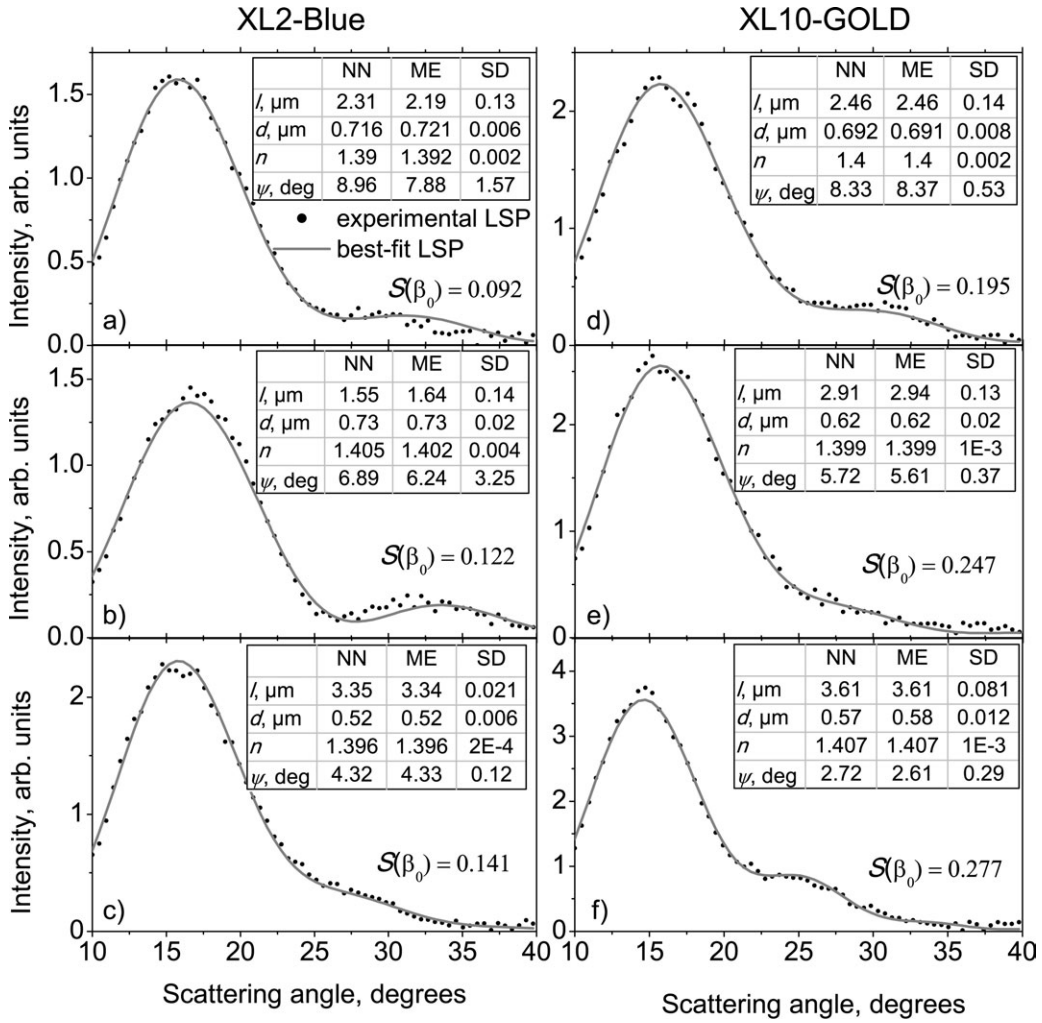

Figure 3. Typical results of global optimization for experimental *E. coli* LSPs, depicting weighted experimental and best-fit database LSPs: *E. coli* XL2-Blue (**a—c**) and *E. coli* XL10-GOLD (**d—f**). Characteristics of a cell that corresponds to the nearest (best-fit) LSP from the database (NN), mathematical expectation (ME) and standard deviation (SD) of parameters are shown in figure tables.

of LSP points (in the range of θ from 10° to 40°), and $w(\theta)$ is weighting function to reduce an effect of the noise on the fitting results (22):

$$w(\theta) = \frac{1^\circ}{\theta}\exp\left(-2\ln^2(\theta/54^\circ)\right). \quad (3)$$

Global minimization is performed by the nearest-neighbor interpolation using a precomputed database of 80,000 theoretical LSPs (36). Model parameters corresponding to the theoretical LSPs were chosen randomly from the ranges $l \in [1.2, 8.0]$ μm, $d \in [0.5, 1.2]$ μm, $n \in [1.39, 1.41]$, $\psi \in [0^\circ, 30^\circ]$, which amply cover the range of *E. coli* cells of the studied strains. For the refractive index, we advisedly selected a relatively narrow range of [1.39, 1.41] using existing information on refractive index for *E. coli* cells (37–40) to overcome the problem of parameter compensation (36). In other words, we restrict the additional information on refractive index obtained from the experimental LSP (because original bounds are already tight), but significantly increase the accuracy of measurement of all other bacteria characteristics, especially its length. The range of ψ is based on the hydrodynamic orientation of elongated cells in Poiseuille flow (18), which makes larger values of ψ physically improbable. Total one-time computational effort to calculate the database of LSPs is about 3,000 core-hours on the supercomputer.

Comparing an experimental LSP with all theoretical LSPs from the database, we do not only find the best-fit theoretical LSP with parameters $\boldsymbol{\beta}_0$ that minimizes $S(\boldsymbol{\beta})$, but also obtain an approximate description of the whole surface of $S(\boldsymbol{\beta})$. The latter is used to calculate probability density function $P(\boldsymbol{\beta})$ over parameter space for a given experimental LSP through the Bayesian approach. $P(\boldsymbol{\beta})$ is further used to calculate mathematical expectation $\boldsymbol{\mu} = <\boldsymbol{\beta}>$ (generally different from $\boldsymbol{\beta}_0$), standard deviations of parameter estimates, and 95% highest-posterior density confidence region (see (36) for details). The width Δ of the projection of the latter on a certain parameter

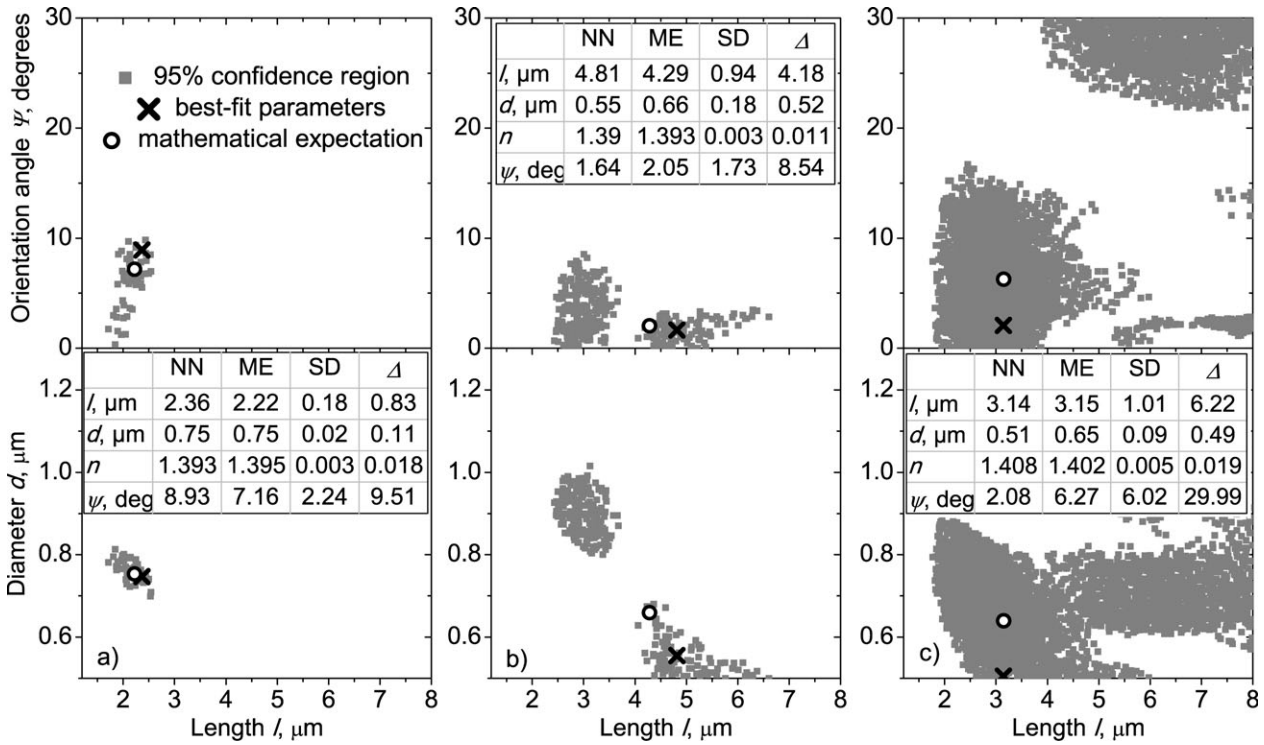

Figure 4. Projections of 95% highest-posterior-density confidence regions for three experimental LSPs with characterization results shown in figure tables: (**a**) normal and (**b**, **c**) abnormal confidence regions. Symbol Δ denotes the width of the confidence range for the corresponding parameter.

is a robust measure of characterization accuracy. Finally, we note that typical processing time for a single measured bacterium is about 0.2 s on a standard desktop computer.

Results

We measured LSPs of individual *E. coli* cells, total 2,918 and 7,367 for XL2-Blue and XL10-GOLD, respectively. The global optimization algorithm described in "Inverse Light-Scattering Problem" section was applied to each cell. Typical results of this procedure for three random bacteria cells from each of two strains are shown in Figures 3a–3c and Figures 3d–3f, respectively. We note that typical results for refractive index are noninformative because for 30% of *E. coli* cells the 95% confidence range (± two standard deviations) covers the whole range used for database construction (Fig. 3b). This agrees with the design goal of characterization method (see "Inverse Light-Scattering Problem" section).

In both samples, we have discovered a subpopulation of bacteria with unacceptably large characterization errors. This is best illustrated by the confidence regions in coordinates of the length, diameter, and orientation angle, which consist of two or more separated domains—typical example is shown in Figures 4b and 4c. The corresponding bacteria are characterized by high values of confidence range width: $\Delta\psi$, Δr, and Δl, as illustrated by the corresponding maps (Fig. 5), and large standard errors of length, diameter, and orientation angle. For the comparison, the typical normal confidence region is shown in Figure 4a. Discontinuous confidence regions appear due to combination of factors that deform measured LSP, including imperfect alignment of SFC and deviation of a realistic shape from the used model, and peculiar dependence of the LSP on model parameters.

Because maps of $\Delta\psi$ versus Δl, Δd versus Δl (Fig. 5) allow unambiguous discrimination of normal and large-error events, we choose this criterion to remove the bacteria with $\Delta\psi > 20^\circ$, $\Delta l > 2$ μm, and $\Delta r > 0.15$ μm from further consideration (at least one of this condition). In other words, only the cells satisfying both gates G1 and G2 remain (Fig. 5), which constitute 38% and 17% of the original samples for XL2-Blue and XL10-Gold, respectively (1,104 and 1,235 cells, respectively). Because experimental deformations do not depend on model parameters, such a filter should not introduce a bias into the distribution of the whole bacteria population over the model parameters. For the remaining bacteria, the median uncertainty (precision) of determined length and diameter is 135 nm and 15 nm, respectively.

The characterization results for each strain are presented as distributions over length and diameter (best-fit values) in Figure 6 in comparison with corresponding distributions obtained with the optical microscopy (see "Optical Microscope" section), showing a good agreement. Moreover, our results fall within the typical ranges reported for other *E. coli* strains for the length (9–11,41) and diameter (10,11). The only significant difference is a minor fraction of cells from XL-10 GOLD sample, for which the SFC-measured diameter

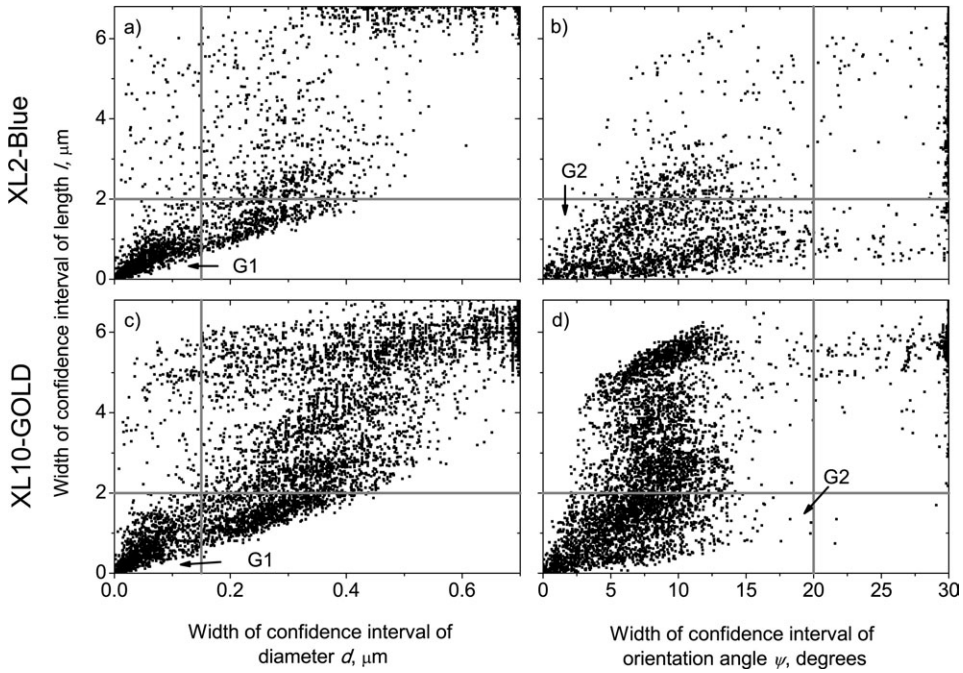

Figure 5. Maps over width of confidence ranges of parameters diameter versus length (**a**, **c**) and orientation angle versus length (**b**, **d**) for two *E. coli* strains: XL2-Blue (a, b) and XL10-GOLD (c, d). Vertical and horizontal lines define gates G1 and G2; only the cells passing both gates are considered for further analysis.

is unusually small (close to 0.5 μm), which is caused by relatively large uncertainties of diameter determination (median is 25 nm) for these particular cells. Also, distributions over SFC-measured parameters are narrower (inside the main mode of the distributions) due to performed gating strategy, which leaves the more accurately characterized part of events, although still representative of the whole population. By contrast, the uncertainty of microscopy measurements is larger

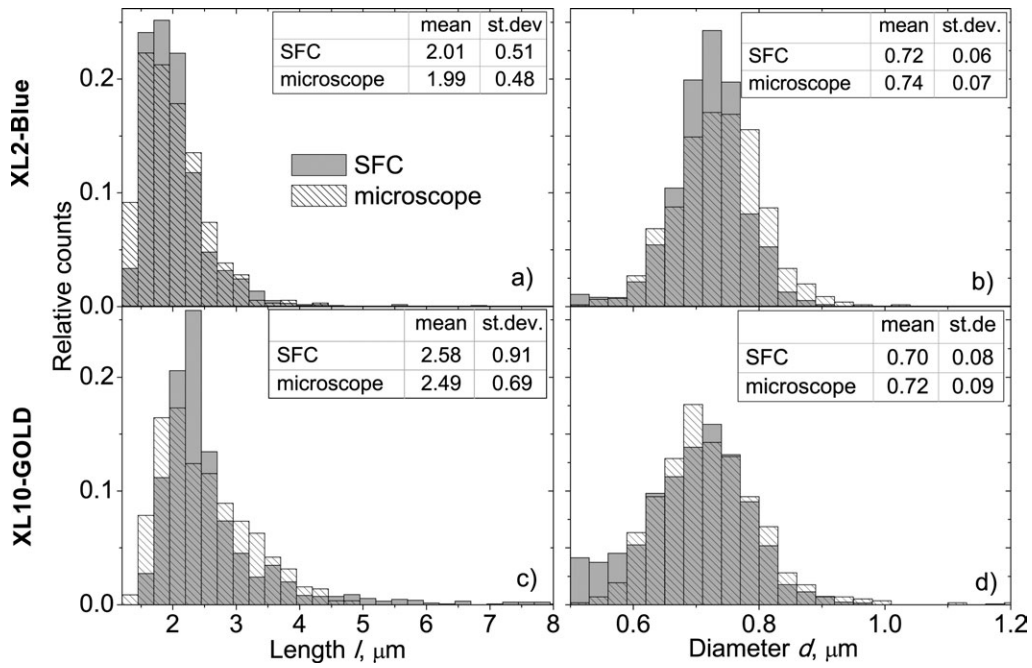

Figure 6. Distributions of XL2-Blue (top) and XL10-GOLD (bottom) *E. coli* strains over length (**a** and **c**, respectively) and diameter (**b** and **d**, respectively) determined from SFC measurements (best-fit values) and obtained with optical microscopy. Mean and standard deviation of these values over the sample are also shown.

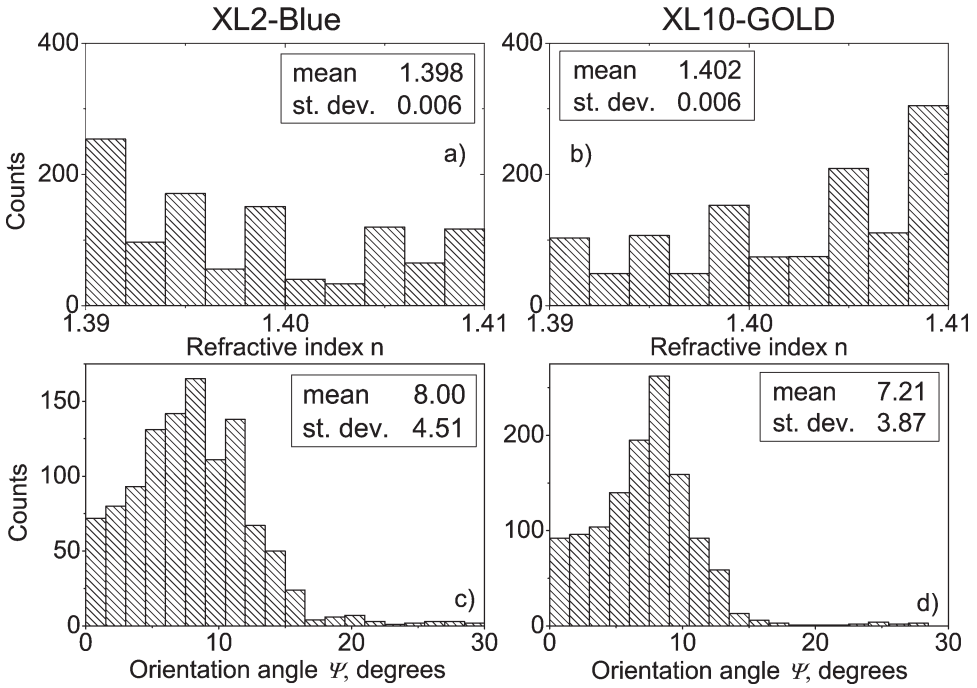

Figure 7. Distributions of XL2-Blue (left column) and XL10-GOLD (right column) *E. coli* strains over refractive index (top) and orientation angle (bottom). Mean and standard deviation of these values over the sample are also shown.

(about 250 nm), which results in broadening of distributions near its mean values. The absence of large bacteria in distributions obtained with optical microscopy is caused by features of the computer program used for processing of microscope images, as described in "Optical Microscope" section, whereas the SFC measurements confirm the presence of these cells in populations.

Distributions over refractive index and orientation angle obtained from the characterization results are presented in Figure 7. One can see that results for refractive index (Figs. 7a and 7b) are noninformative, spanning the whole range that was originally chosen for database construction. This is consistent with single-cell results discussed above.

Discussion

This article describes a new method for characterization of *E. coli* morphology, which allows high-precision determination of length and diameter of single bacteria in a flow from angle-resolved LSPs measured with SFC. We modeled *E. coli* as a cylinder capped with hemispheres and used the DDA to calculate a database of their LSPs in a wide range of model parameters. To solve the ILS problem, we performed the nearest-neighbor interpolation on this database. This allowed us to calculate the probability density function over parameter ranges for a given experimental LSP and to estimate the mathematical expectations and standard deviations for each model parameter. Single-cell measurements allow one to reliably measure the whole distribution of the *E. coli* sample over morphological characteristics.

The method was applied to two strains of *E. coli* cells, showing 135 and 15 nm median precision in determination of length and diameter of single cells, respectively, which is very good for optical methods. We also compared population distributions over model parameters to optical microscope measurements and obtained good agreement for both diameter and length. Unfortunately, the method does not allow the determination of refractive index of individual cells, thus we could not narrow the confidence range based on the literature data.

It is important to note that the SFC-based method is not specific to *E. coli* and can be directly applied to any rod-shaped bacteria. The only additional effort may be needed for extension of the database to larger or smaller bacteria sizes. Therefore, this method is promising for precise control of bacteria morphology during cell cycle studies or for monitoring changes in cell growth rates due to external affects.

Acknowledgments

E.A. Uvarova and V.S. Fishman (Institute of Cytology and Genetics, Novosibirsk, Russia) have kindly provided the studied *E. coli* strains. We also thank Susann Muller and two anonymous reviewers for helpful comments on this manuscript.

Literature Cited

1. Wyatt PJ. Differential light scattering: A physical method for identifying living bacterial cells. Appl Opt 1968;7:1879–1896.
2. Harding SE. Applications of light scattering in microbiology. Biotechnol Appl Biochem 1986;8:489–509.
3. Fouchet P, Jayat C, Hechard Y, Ratinaud MH, Frelat G. Recent advances of flow cytometry in fundamental and applied microbiology. Biol Cell 1993;78:95–109.
4. Diaspro A, Radicchi G, Nicolini C. Polarized light scattering: A biophysical method for studying bacterial cells. IEEE Trans Biomed Eng 1995;42:1038–1043.

5. Maltsev VP, Semyanov KA. Characterisation of Bio-Particles from Light Scattering. Utrecht: VSP; 2004. 132 p.
6. Xu M, Katz A. Statistical interpretation of light anomalous diffraction by small particles and its applications in bio-agent detection and monitoring. In: Kokhanovsky AA, editor.Light Scattering Reviews 3. Springer: Heidelberg; 2008. pp 27–67.
7. Murray J, Hukins DW, Evans P. Application of Mie theory and cubic splines to the representation of light scattering patterns from bacteria in the logarithmic growth phase. Phys Med Biol 1979;24:408–415.
8. Cross DA, Latimer P. Angular dependence of scattering from *Escherichia coli* cells. Appl Opt 1972;11:1225–1228.
9. Bronk BV, Van de Merwe WP, Stanley M. In vivo measure of average bacterial cell size from a polarized light scattering function. Cytometry 1992;13:155–162.
10. Bronk BV, Druger SD, Czégé J, Van de Merwe WP. Measuring diameters of rod-shaped bacteria in vivo with polarized light scattering. Biophys J 1995;69:1170–1177.
11. Van De Merwe WP, Czégé J, Milham ME, Bronk BV. Rapid optically based measurements of diameter and length for spherical or rod-shaped bacteria in vivo. Appl Opt 2004;43:5295–5302.
12. Allman R, Hann AC, Manchee R, Lloyd D. Characterization of bacteria by multiparameter flow cytometry. J App Microbiol 2008;73:438–444.
13. Steen HB, Boye E, Skarstad K, Bloom B, Godal T, Mustafa S. Applications of flow cytometry on bacteria: Cell cycle kinetics, drug effects, and quantitation of antibody binding. Cytometry 1982;2:249–257.
14. Boye E, Steen HB, Skarstad K. Flow cytometry of bacteria: A promising tool in experimental and clinical microbiology. J Gen Microbiol 1983;129:973–980.
15. Müller S, Nebe-von-Caron G. Functional single-cell analyses: Flow cytometry and cell sorting of microbial populations and communities. FEMS Microbiol Rev 2010;34:554–587.
16. Rajwa B, Venkatapathi M, Ragheb K, Banada PP, Hirleman ED, Lary T, Robinson JP. Automated classification of bacterial particles in flow by multiangle scatter measurement and support vector machine classifier. Cytometry Part A 2008;73A:369–379.
17. Venkatapathi M, Rajwa B, Ragheb K, Banada PP, Lary T, Robinson JP, Hirleman ED. High speed classification of individual bacterial cells using a model-based light scatter system and multivariate statistics. Appl Opt 2008;47:678–686.
18. Maltsev VP. Scanning flow cytometry for individual particle analysis. Rev Sci Instrum 2000;71:243–255.
19. Strokotov DI, Moskalensky AE, Nekrasov VM, Maltsev VP. Polarized light-scattering profile—advanced characterization of nonspherical particles with scanning flow cytometry. Cytometry Part A 2011;79A:570–579.
20. Shvalov AN, Surovtsev IV, Chernyshev AV, Soini JT, Maltsev VP. Particle classification from light scattering with the scanning flow cytometer. Cytometry 1999;37:215–220.
21. Fiorani L, Maltsev VP, Nekrasov VM, Palucci A, Semyanov KA, Spizzichino V. Scanning flow cytometer modified to distinguish phytoplankton cells from their effective size, effective refractive index, depolarization, and fluorescence. Appl Opt 2008;47:4405–4412.
22. Strokotov DI, Yurkin MA, Gilev KV, van Bockstaele DR, Hoekstra AG, Rubtsov NB, Maltsev VP. Is there a difference between T- and B-lymphocyte morphology? J Biomed Opt 2009;14:064036–064048.
23. Konokhova AI, Yurkin MA, Moskalensky AE, Chernyshev AV, Tsvetovskaya GA, Chikova ED, Maltsev VP. Light-scattering flow cytometry for identification and characterization of blood microparticles. J Biomed Opt 2012;17:057006–057014.
24. Shvalov AN, Soini JT, Surovtsev IV, Kochneva GV, Sivolobova GF, Petrov AK, Maltsev VP. Individual *Escherichia coli* cells studied from light scattering with the scanning flow cytometer. Cytometry 2000;41:41–45.
25. Bartholomew-Biggs MC, Ulanowski ZJ, Zakovic S. Using global optimization for a microparticle identification problem with noisy data. J Glob Opt 2005;32:325–347.
26. Li W, Jaffe JS. Sizing homogeneous spherical particles from intensity-only angular scatter. J Opt Soc Am A 2010;27:151–158.
27. Kolesnikova IV, Potapov SV, Yurkin MA, Hoekstra AG, Maltsev VP, Semyanov KA. Determination of volume, shape and refractive index of individual blood platelets. J Quant Spectrosc Radiat Transfer 2006;102:37–45.
28. Yurkin MA, Semyanov KA, Tarasov PA, Chernyshev AV, Hoekstra AG, Maltsev VP. Experimental and theoretical study of light scattering by individual mature red blood cells by use of scanning flow cytometry and discrete dipole approximation. Appl Opt 2005;44:5249–5256.
29. Bohren CF, Huffman DR. Absorption and Scattering of Light by Small Particles, 1st ed. New York: Wiley; 1983. 544 p.
30. Sliusarenko O, Heinritz J, Emonet T, Jacobs-Wagner C. High-throughput, subpixel precision analysis of bacterial morphogenesis and intracellular spatio-temporal dynamics. Mol Microbiol 2011;80:612–627.
31. Protocol for the preparation of LB liquid media and agar plates with Ampicillin. Available at:http://www.goldbio.com/pdf/543-Protocol1.pdf (last accessed 29.03.2013).
32. Yurkin MA, Hoekstra AG. The discrete dipole approximation: An overview and recent developments. J Quant Spectrosc Radiat Transfer 2007;106:558–589.
33. Yurkin MA, Hoekstra AG. The discrete-dipole-approximation code ADDA: Capabilities and known limitations. J Quant Spectrosc Radiat Transfer 2011;112:2234–2247.
34. Supercomputing Center of the Novosibirsk State University. Available at:http://nsu.ru (last accessed 29.03.2013).
35. Begg KJ, Donachie WD. Cell shape and division in *Escherichia coli*: Experiments with shape and division mutants. J Bacteriol 1985;163:615–622.
36. Moskalensky AE, Yurkin MA, Konokhova AI, Strokotov DI, Nekrasov VM, Chernyshev AV, Tsvetovskaya GA, Chikova ED, Maltsev VP. Accurate measurement of volume and shape of resting and activated blood platelets from light scattering. J Biomed Opt 2013;18:017001–017012.
37. Bateman JB, Wagman J, Carstensen EL. Refraction and absorption of light in bacterial suspensions. Colloid Polym Sci 1966;208:44–58.
38. Bryant FD, Seiber BA, Latimer P. Absolute optical cross sections of cells and chloroplasts. Arch Biochem Biophys 1969;135:97–108.
39. Waltham C, Boyle J, Ramey B, Smit J. Light scattering and absorption caused by bacterial activity in water. App Opt 1994;33:7536–7540.
40. Balaev AE, Dvoretski KN, Doubrovski VA. Refractive index of *Escherichia coli* cells. SPIE Proc 2002;4707:253–260.
41. Cullum J, Vicente M. Cell growth and length distribution in *Escherichia coli*. J Bacteriol 1978;134:330–337.